Mon. Not. R. Astron. Soc. **000**, 000–000 (0000) Printed 26 July 2018 (MN LATEX style file v2.2)

An inefficient dwarf: Chemical abundances and the evolution of the Ursa Minor dwarf spheroidal galaxy

Uğur Ural[1], Gabriele Cescutti[1], Andreas Koch[2], Jan Kleyna[3], Sofia Feltzing[4], Mark I. Wilkinson[5]

[1]*Leibniz Institut für Astrophysik Potsdam (AIP), An der Sternwarte 16, 14482 Postdam, Germany*
[2]*Landessternwarte, Zentrum für Astronomie der Universität Heidelberg, Königstuhl 12, 69117 Heidelberg, Germany*
[3]*Institute for Astronomy (IfA), University of Hawaii, 2680 Woodlawn Drive, Honolulu, HI, 96822, USA*
[4]*Lund Observatory, Department of Astronomy and Theoretical Physics, Box 43, 22100 Lund, Sweden.*
[5]*Department of Physics and Astronomy, University of Leicester, University Road, Leicester, LE1 7RH, United Kingdom .*
Accepted for publication in MNRAS

arXiv:1502.04133v1 [astro-ph.GA] 13 Feb 2015

26 July 2018

ABSTRACT

We present detailed chemical element abundance ratios of 17 elements with $8 \leqslant Z \leqslant 60$ in three metal poor stars in the Ursa Minor dwarf spheroidal galaxy, which we combine with extant data from the literature to assess the predictions of a novel suite of galaxy chemical evolution models. The spectroscopic data were obtained with the Keck/HIRES instrument and revealed low metallicities of [Fe/H]=−2.12, −2.13 and −2.67 dex. While the most metal poor star in our sample shows an overabundance of [Mn/Fe] and other Fe-peak elements, our overall findings are in agreement with previous studies of this galaxy: elevated values of the [α/Fe] ratios that are similar to, or only slightly lower than, the halo values but with SN Ia enrichment at very low metallicity, as well as an enhancement of the ratio of first to second peak neutron capture elements [Y/Ba] with decreasing metallicity. The chemical evolution models which were tailored to reproduce the metallicity distribution function of the dSph, indicate that UMi had an extended star formation which lasted nearly 5 Gyr with low efficiency and are able to explain the [Y/Ba] enhancement at low metallicity for the first time. In particular, we show that the present day lack of gas is probably due to continuous loss of gas from the system, which we model as winds.

Key words: galaxies: individual (UMi I dSph)–galaxies: dwarf–galaxies: chemistry and star formation history—Local Group—galaxies: abundances—galaxies: evolution

1 INTRODUCTION

The increasing number of detailed spectroscopic surveys investigating kinematic and chemical properties of dwarf spheroidal (dSph) galaxies (see e.g., Tolstoy et al. 2004; Helmi et al. 2006; Koch et al. 2006; Martin et al. 2007; Walker et al. 2009a) provide new opportunities to study their local formation environment in detail and the formation and evolution of galaxies in general. Despite their low luminosities, their gravitational potentials had to be large enough to confine their gas for sufficient time to allow an extended period of star formation (SF) to occur. This is indicated by the large spreads in their metallicities and by the presence of stellar populations as young as 1-2 Gyr (Tolstoy et al. 2009, and references therein), even down to 200 Myr (Stetson et al. 1998; de Boer et al. 2012). Samples of even a few stars in faint dSphs can provide interesting information (Koch et al. 2008; Simon et al. 2010) as they emphasise the diversity of the chemical inventories of individual dSphs and guide us through the processes that affected their evolution (Tolstoy et al. 2009).

One of the most important observed signatures is the spread in the ratio of [α/Fe] in dSphs where the downturn of [α/Fe] with increasing metallicity marks the time scale on which SN Ia started to contribute to the enrichment of the interstellar medium (ISM). Other mechanisms such as episodic SF (Hendricks et al. 2014) or a change in the Initial Mass Function (IMF) where the very massive stars do not occur (McWilliam et al. 2013) might also be responsible for the spread found in the abundances of the α-elements in the present day dSphs.

Although many isolated dwarf galaxies seem to be dominated by exclusively old and/or young stellar populations (Benítez Llambay et al. 2014), among the dSphs, Ursa Minor (UMi) is a rare system which has exclusively old stars and hence a

Target	I	V	K	α J2000	δ (J2000)	T_{eff} (phot)	T_{eff} (spec)	log g	v_{mic}	[Fe/H]	v_r (km s^{-1})
UMI718	16.30	17.46	14.967	15:02:25.58	66:55:25.39	4563	4540	1.1	2.25	-2.12	-247.6
UMI396	15.59	16.94	14.018	15:05:52.04	66:41:30.05	4312	4290	0.5	2.35	-2.13	-228
UMI446	16.96	18.07	15.131	15:02:01.53	66:49:22.36	4640	4580	1.6	2.80	-2.67	-246

Table 1. Observed stars: The K magnitudes are obtained from 2MASS photometry while I and V are from Kleyna et al. (1998). The preliminary estimates for the photometric temperature T(phot) from (V−I) and the surface gravity are calculated assuming a metallicity of [Fe/H]= −2 dex, mass of 0.8$M_\odot$ and distance of 68 kpc.The T(spec), log g, v_{mic} and [Fe/H] are the values found by iteration of the best atmospheric models used to calculate the spectroscopic abundances (see text for details).

candidate for being a dSph similar to those which contributed to the growth of the outer halo. Carrera et al. (2002) suggested that 95% of its stars are older than 10 Gyrs and Ikuta & Arimoto (2002) constrain the duration of SF in UMi to be between 3.9 to 6.5 Gyr. In this paper, we add the chemical abundances of three red giant branch stars in UMi to the eighteen stars from the previous studies by Cohen & Huang (2010); Shetrone et al. (2001); Sadakane et al. (2004); Kirby & Cohen (2012). The chemical evolution models tested by Kirby et al. (2011) and Kirby et al. (2013) showed that the metallicity distribution function (MDF) of UMi can only be explained with models without extended infall of gas. We present detailed chemical evolution models describing the nucleosynthesis of 12 elements for the combination of our new data set with the extant data, examine these findings and study the implications for individual elements.

The paper is organised as follows: In Section 2, both the observations and the methods used to obtain the chemical abundances are explained and the final abundances for α, Fe-peak and neutron capture elements are given for three new stars. In Section 3, we explain the details of our chemical evolution models and compare them to the combined data set. In Section 4, we discuss our results and open questions.

2 OBSERVATIONS AND ANALYSIS

2.1 Observations and data reduction

The observations were made using the High Resolution Echelle Spectrograph (HIRES; Vogt et al. (1994)) on the Keck telescope on the night of UT 2006-06-05. The targets were selected from legacy KPNO 4 m MOSAIC imaging as in Wilkinson et al. (2004). Details of the targets are given in Table 1, together with some of their basic characteristics.

We used HIRES configured with the red collimator, the B2 decker set for a fully open slit, the kv408 filter with the cut off at 450 nm, an echelle angle of 0âŮę.11197 and cross-disperser angle of 0âŮę.65899. We obtained a full wavelength coverage of 440-750 nm with a 10 nm wide gap at 590 nm. The exposure times were 4000s for UMI718, 3600s for UMI396 and 3000s for UMI446.

The raw data were reduced using the MAKEE data reduction package[1], which performs standard steps such as bias and flat field corrections, wavelength calibration via Th-Ar lamps, optimal subtraction, and sky subtraction. This procedure resulted in signal-to-noise (S/N) ratios measured in the H_α order around 660 nm of 25, 30, 12 per pixel, respectively, for UMI718, UMI396 and UMI446.

X	λ [Å]	E.P. [eV]	log gf	EW [mÅ]		
				UMI396	UMI718	UMI446
O	6300.31	0.00	−9.780	34.6	-	-
Mg	4571.10	0.00	−5.623	-	123.6	93.5
Mg	4702.99	4.34	−0.440	98.9	111.2	91.1
Mg	5528.41	4.34	−0.498	132.4	107.8	-
Mg	5711.09	4.34	−1.724	36.3	-	-
Si	7423.50	5.62	−0.314	30.8	-	-
Ca	4435.69	1.89	−0.519	-	-	72.7
Ca	4454.78	1.90	0.260	-	116.0	-

Table 2. Equivalent width measurements. Columns are: (I) Element; (2) Wavelength of the absorption line; (3) Excitation energy of the lower energy level; (4) Oscillator strength; (5,6,7) Equivalent width of the line measured for each star. This table is available in its entirety in the electronic version of the Journal.

The continuum fit to each echelle order was obtained by dividing by high-order polynomials within the `continuum` task in IRAF[2]. Subsequently, the velocity correction from vacuum to air velocities was made using the `disptrans` utility and the Doppler shift was computed from the average wavelength shift of a few of the strongest lines in several orders. These velocities are given in Table 1.

2.2 Stellar parameters and abundance calculations

We derived chemical element abundances via a standard equivalent widths (EWs) analysis that closely follows the procedures used in our previous works (e.g. Koch et al. 2009). All analyses employed the 2010 version of the stellar line analysis code MOOG (Sneden 1973). The EWs of the absorption lines were measured within the `splot` task in IRAF assuming a Gaussian line profile. The line list was assembled from Moore et al. (1966) combined with the log gf values from the Kurucz database. The EWs for all the lines used in our analysis are given in Table 2. In order to avoid saturation or spurious, weak lines, we conservatively excluded all Fe I and Fe II lines with EW$\geqslant$160mÅ and EW$\leqslant$40mÅ from our analysis.

Although we do not expect the effect of hyperfine splitting to be large in our spectra, they were investigated in the derivation of abundance ratios for Sc, Mn, Cu, and Ba, using wavelengths and log gf values taken from the Kurucz database with the exceptions of the Sc II line at 467.0 from McWilliam et al. (1995) and 565.7, and 568.4 nm, calculated with the coefficients from Johnson (2002). Except for the larger corrections for [Mn/Fe], which ranged from 0.09 to 0.15 dex, the inclusion of hyperfine splitting causes

[1] MAKEE was developed by T. A. Barlow specifically for reduction of Keck HIRES data. It is freely available on the World Wide Web at the Keck Observatory home page, `http://www2.keck.hawaii.edu/inst/hires/makeewww`

[2] IRAF is distributed by the National Optical Astronomy Observatory, which is operated by the Association of Universities for Research in Astronomy (AURA) under cooperative agreement with the National Science Foundation

only small changes in the abundances of the other elements. Barium (scandium) were corrected by 0.05 (0.06) dex in UMI718, 0.01 (0.03) dex in UMI396 and 0.02 (0.02) dex in UMI446. The copper abundance differed only in UMI718 (by 0.03 dex) with the inclusion of hyperfine splitting.

Apart from a Non-LTE correction applied to the Al/Fe abundance by Cohen & Huang (2010), all of the data used in this paper are based on the assumption of LTE conditions. Our stars do not show any signs of ionisation imbalance in the abundances we calculate for Fe and Ti within the uncertainties. The calculations of Bergemann & Gehren (2008) for Cr and Bergemann & Cescutti (2010) for Mn imply upward-corrections by ∼0.4 dex in these elements, but we note that their parameter range mainly included dwarf stars and did not extend to cool giants as in our sample. Thus we refrain from applying these corrections to these elements in the following.

The initial estimates for the temperature and the surface gravity listed in Table 1 are the photometric values based on V-I, using the calibration of Ramírez & Meléndez (2005), where we adopted a reddening of E(B-V)=0.02 (Schlegel et al. 1998) and an initial guess for the metallicity of [Fe/H] = −2.0. Throughout our analysis, we constructed model atmospheres for a large range of metallicities and microturbulent velocities by interpolation of Kurucz's[3] grid of one-dimensional 72-layer, plane-parallel, line-blanketed models without convective overshoot, assuming local thermodynamic equilibrium (LTE) for all species. For the UMi stars, we incorporated the opacity distribution functions ODFNEW described by (Castelli & Kurucz 2003)[4]. As UMI446 was found to be very metal poor, we tested our final results with the α enhanced AODFNEW models as well but found that these did not affect the results more than 0.01 dex for any of the elements.

These model atmospheres were then used in MOOG, together with the EWs to calculate the abundances of the Fe I and Fe II lines for each star. The iteration to obtain the best model parameters was made first by checking the abundance trends with excitation potential in order to estimate the spectroscopic temperature and removing any trends with the reduced EW to estimate the microturbulence velocity. Finally, the best value for the surface gravity was measured by minimising the [Fe I/Fe II] ratio. During this procedure, all steps were iterated to convergence. Furthermore, we excluded strong lines with EW⩾160 to avoid saturated lines, and EW⩽40mÅ to avoid biasses due to low S/N (e.g., Magain 1984), from this part of the analysis. Although it is difficult to calculate formal errors for the temperature, log g and microturbulence as these parameters are highly interdependent (though see Section 2.3), our final models minimised the correlation coefficients for all of these (less than 6% for T and V for all of our stars), and we could achieve a reasonable ionization balance solution, where the difference between the abundances of Fe I and Fe II are 0.07, 0.05, and 0.03 dex for UMI718, UMI396 and UMI446 respectively.

In a few cases where the number of measured lines were very small for an element, we included lines with EW<40mÅ if the lines were clear and without blends. These exceptional, weaker lines ([Ce/Fe] for UMI718, [Si/Fe], [Cr II/Fe II] and [Ce/Fe] for UMI396, [Cu/Fe], [Y/Fe] and [Nd/Fe] for UMI446) were rechecked during the iterative process of finding the stellar atmosphere parameters which were normally adjusted through the trends seen for the [Fe/H] abundances. Despite the very low S/N in UMI446, there were features strong enough to be measured in both blue and red parts of the spectra.

[3] http://kurucz.harvard.edu

[4] www.stsci.edu/hst/observatory/crds/castelli_kurucz_atlas.html

Model	Description	Infall	Galactic winds	Final stellar mass [$M_\odot$]	M_o [$M_\odot$]
A	Closed box	No	No	$\sim 2.3\times10^5$	1.2×10^7
B	Accretion	Yes	No	$\sim 2\times10^5$	2.4×10^7
C	Acc + winds	Yes	Yes	$\sim 2\times10^5$	2.4×10^7

Table 4. The parameters in the chemical evolution models. M_o is the gas mass used in eq. 2, and the laws for gas infall and galactic winds are given in eq. 2 and eq. 3, respectively.

2.3 Chemical abundance measurements and uncertainties

By varying the model atmosphere parameters by their typical uncertainties of 100K (T) and 0.2 km/s (v_{mic}), we find the systematic errors in [Fe/H] to be 0.1 dex for UMI718, 0.15 dex for UMI718 and 0.13 dex for UMI446.

The abundances calculated for 17 elements in our observed UMi stars are presented in Table 3, together with the Solar abundance scale, which was adopted from Asplund et al. (2009). The detailed comparison with previous data and our chemical evolution models are presented in Section 3.

The overall abundance errors for each element given in Table 3 are determined by using $\sigma/\sqrt{N}$ where σ is the standard deviation of the individual line abundances and N is the number of observed lines for this element. In Table 3 we list each of these values.

Similarly to the Kirby & Cohen (2012) data, UMI446 and UMI718 have radial velocities which make the telluric absorption lines coincide exactly with the forbidden oxygen line at 630.03 nm. Therefore, this line was only measured in UMI396 by fitting synthetic spectra.

3 ABUNDANCES AND THE CHEMICAL EVOLUTION MODELS FOR URSA MINOR

In this section, we present the chemical abundances calculated for 17 elements in three new UMi stars (see Table 3) and use a set of homogeneous chemical evolution models to investigate the implications of the abundances in a data set comprising both our new data and those obtained in previous studies of UMi. The main characteristics of our models are summarised in Table 4. The difference among the models is the treatment of the gas flows. Model A is a closed box, without infall or outflow; model B has infall but no galactic winds; in model C, we take into account both infall and galactic winds. We constrain our models to follow the observational SF given by Carrera et al. (2002), while imposing a star formation law given by

$$\psi(t)[10^{-4}\mathrm{M}_\odot/\mathrm{yr}] = \left\{ \begin{array}{ll} \left[3\cdot10^{-2}M_{\rm gas}(t)N^{\sigma,t_0}(t) & \\ \qquad -10^{-10}t+0.5\right] & \text{if t} \leqslant 5\text{Gyr} \\ 0 & \text{if t} > 5\text{Gyr} \end{array} \right\} \quad (1)$$

where, N^{σ,t_0} is a normalized Gaussian function with σ of 0.5 Gyr, centered at t_0 equal to 0.5 Gyr. The SF law provided by Eq. 1 mimics the observed peak of early SF with a subsequent period of extended SF with lower efficiency, which stops after 5 Gyr as proposed by Carrera et al. (2002).

	SUN		UMI718			UMI396			UMI446	
X	$\log\epsilon(X)_\odot$	$\log\epsilon(X)$	σ(nr of lines)	[X/Fe]	$\log\epsilon(X)$	σ(nr of lines)	[X/Fe]	$\log\epsilon(X)$	σ(nr of lines)	[X/Fe]
Fe I	7.5	5.38	0.17(88)	-2.12±0.02	5.37	0.19 (118)	-2.13±0.02	4.83	0.26(68)	-2.67±0.03
Fe II	7.5	5.45	0.19(5)	-2.05±0.08	5.42	0.17(6)	-2.08±0.07	4.86	0.19(7)	-2.64±0.07
O I synt	8.69	-	-	-	6.99	...(1)	0.38 ± 0.13	-	-	-
Mg I	7.6	5.74	0.09(3)	0.26 ± 0.05	5.79	0.15(3)	0.32 ± 0.08	5.26	0.10(2)	0.33 ± 0.08
Si I synt	7.51	-	-	-	5.57	...(1)	0.19 ± 0.13	-	-	-
Ca I	6.34	4.55	0.34(15)	0.33 ± 0.09	4.35	0.15(16)	0.14 ± 0.04	3.97	0.20(7)	0.3 ± 0.08
Sc II∗	3.15	1.14	0.09(3)	0.02 ± 0.09	1.08	0.19(4)	−0.02 ± 0.12	1.15	0.27(3)	0.63 ± 0.18
Ti I	4.95	2.96	0.16(15)	0.13 ± 0.04	2.86	0.19(25)	0.04 ± 0.04	2.73	0.23(7)	0.45 ± 0.09
Ti II	4.95	3.07	0.09(15)	0.17 ± 0.08	3.06	0.15(17)	0.19 ± 0.08	2.79	0.34(13)	0.48 ± 0.12
Cr I	5.64	3.50	0.18(12)	−0.02 ± 0.05	3.27	0.09(13)	−0.24 ± 0.03	2.99	0.07(6)	0.02 ± 0.04
Cr II∗	5.64	-	-	-	3.33	...(1)	−0.23 ± 0.13	-	-	-
Mn I∗	5.43	3.16	0.17(5)	−0.15 ± 0.08	2.96	0.12(3)	−0.35 ± 0.08	3.05	0.19(3)	0.29 ± 0.1
Ni I	6.22	4.24	0.17(17)	0.14 ± 0.04	4.11	0.17(24)	0.02 ± 0.03	3.87	0.11(5)	0.32 ± 0.05
Cu I∗∗	4.19	1.92	...(1)	−0.18 ± 0.1	-	-	-	1.64	...(1)	0.12 ± 0.34
Zn I	4.56	2.41	0.12(2)	−0.03 ± 0.08	2.54	...(1)	0.11 ± 0.13	-	-	-
Y II	2.21	−0.32	0.19(3)	−0.48 ± 0.13	−0.35	0.04(3)	−0.48 ± 0.07	−0.23	...(1)	0.18 ± 0.34
Ba II∗	2.19	−0.46	0.1(3)	−0.55 ± 0.1	−0.35	0.08(2)	−0.45 ± 0.09	−1.21	0.47(2)	−0.74 ± 0.34
Ce II∗	1.58	−0.34	0.03(2)	0.13 ± 0.1	−0.65	0.13(2)	−0.15 ± 0.12	-	-	-
Nd II	1.42	-	-	-	−0.68	0.14(3)	−0.02 ± 0.1	−0.31	...(1)	0.89 ± 0.34
Sm II∗∗	0.96	-	-	-	-0.27	0.04(3)	0.9 ± 0.07	-	-	-

Table 3. Abundances of chemical elements in our target UMi stars and the Solar abundance scale, which was adopted from Asplund et al. (2009).(∗) For the values that come from the measurements of a single spectral line, we assume the abundance error to be the same as the largest calculated error for that star (0.1 for UMI718 and UMI396, 0.3 for UMI446). The abundance values are given in columns 5, 8 and 11 in terms of [X/Fe] and [Fe/H] for the Fe I and Fe II. (∗∗)We measure a total Sm II abundance of [Sm/Fe]=0.88 for UMI396, with a surprisingly low standard deviation of 0.04 dex from the lines at 451.96, 452.39 and 456.62 nm. Although interesting, as all three lines are very weak with EW⩽25 and are at the blue end of the spectra, we omit this element in our interpretation of the chemical abundances in UMi.

The infall law used in models B and C takes the same form as the peak of the SF described in Eq.1 and is given by

$$G_{\rm Infall}(t)[M_\odot/yr] = M_o \cdot N^{\sigma,t_0}(t) \quad (2)$$

Models B and C have no initial gas and reach M_o which is given in Table 4 following the infall law given in Eq. 2. Although the infall law is not directly included in the SF law, the common form of these equations provides an implicit connection between the SF and the infall.

The galactic wind for model C has the simple form

$$G_{\rm wind}(t)[10^{-4}M_\odot/yr] = \begin{cases} 0 & \text{if t} \leqslant 2\text{Gyr} \\ 2\cdot 10^{-5}\cdot M_{gas}(t) & \text{if t} > 2\text{Gyr} \end{cases} \quad (3)$$

and is assumed to act only at the end of the gas infall and of the main SF episode (after 2 Gyrs). By implementing the winds with the simplest possible assumptions, we are able to investigate their implication on the chemical evolution, without being forced to constrain their origin(s), given the fact their origins are still not clearly understood.

The top row in Fig. 1 shows the total mass, gas mass and the stellar mass for the three models as a function of time, while in the second row we show the three SF histories obtained for each individual model. As model A, which has all the gas available from the outset, produces stars more efficiently than models B and C, in order to obtain the same final stellar masses in all models, the initial gas mass in models B and C is twice that of model A. Both models A and B have a large amount of gas left at the end, however, and it is clear that the loss of gas through winds is necessary to explain the lack of gas observed in UMi.

In all of our models the IMF of Salpeter (1955) is used, and the other chemical evolution parameters, such as the treatment of SNe Ia, and the nucleosynthesis, as well as the stellar lifetimes are those adopted by François et al. (2004). The exceptions are Mn, for which we follow the nucleosynthesis adopted in Cescutti et al. (2008), and the neutron capture elements Ba and Y, for which we adopt the same nucleosynthesis of model EC+s 2 shown in Cescutti & Chiappini (2014). The latter study assumed that the r-process elements are produced by electron capture SN in stars with masses between $8 - 10M_\odot$ and the s-process elements are produced in rotating massive stars (spinstars) with masses between 15 and $40M_\odot$.

The parameters we assumed aim to reproduce the observed metallicity distribution function (MDF) observed by Kirby et al. (2011). Fig. 2 compares the MDF found in our models with the observed distribution of stellar metallicities. By means of a simplified chemical evolution model, Kirby et al. (2011) already showed that it is not possible to find a model which is able to reproduce the observed MDF without infall. Our findings agree with their conclusions, and indeed our model A only poorly approximates the observed MDF. While our model B (which includes gas infall) is able to match the main characteristics of the observed MDF, as shown by Fig. 1, it cannot explain the absence of gas displayed at the present time by UMi - which is also a common feature of all the dSph galaxies around the Milky Way. The implementation of a galactic wind in Model C, albeit in a simplified manner, solves this problem. We note that it also improves the match of the theoretical MDF with the observed one by slightly extending the tail of the distribution at high metallicity. We emphasize that the MDF and the SF law are the only observational constraints that were used in setting the constants in Eqs. 1,2 and 3. It is then noteworthy that the ensueing chemical evolution model, shown in Figs. 3-7 are successful in

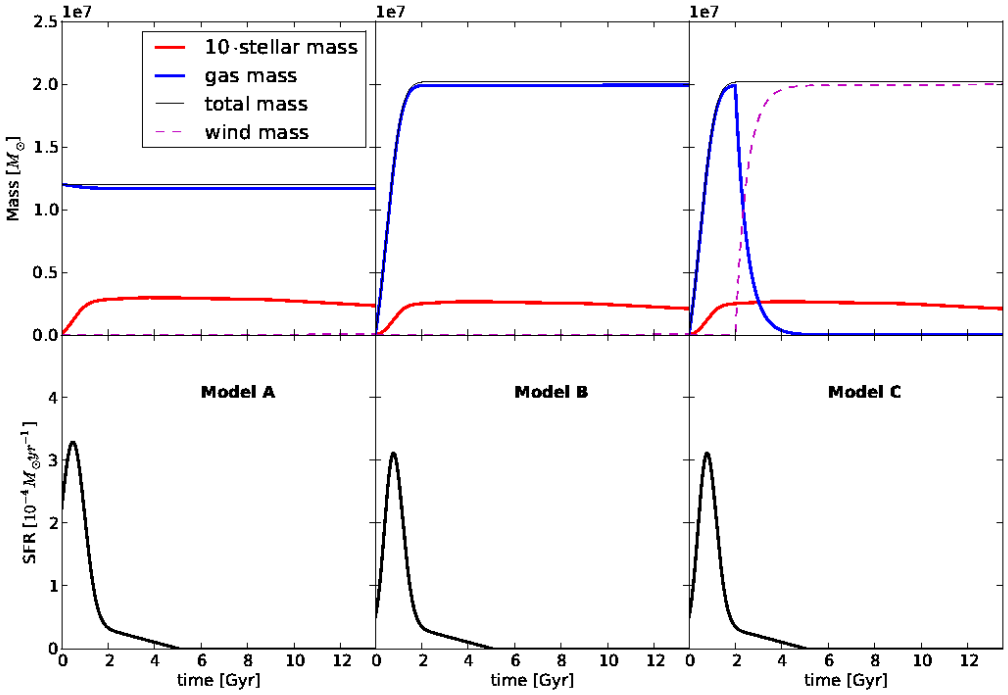


Figure 1. Top: The mass of baryons, gas, stars and wind as functions of time for models A, B and C (from left to right). Bottom: the SF rate as a function of time for the same models.

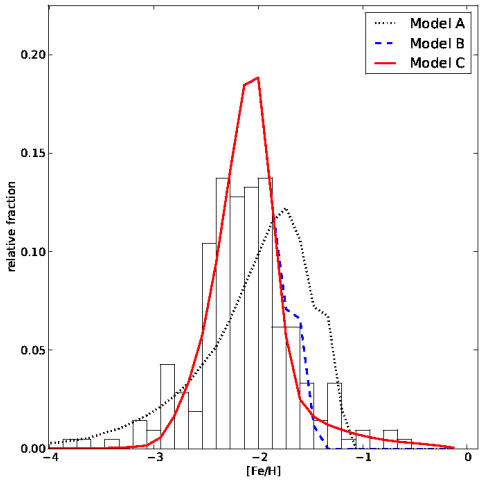


Figure 2. Comparison between the observed MDF histogram (Kirby et al. 2011) and the theoretical MDF produced by our models A (black), B(blue) and C(red).

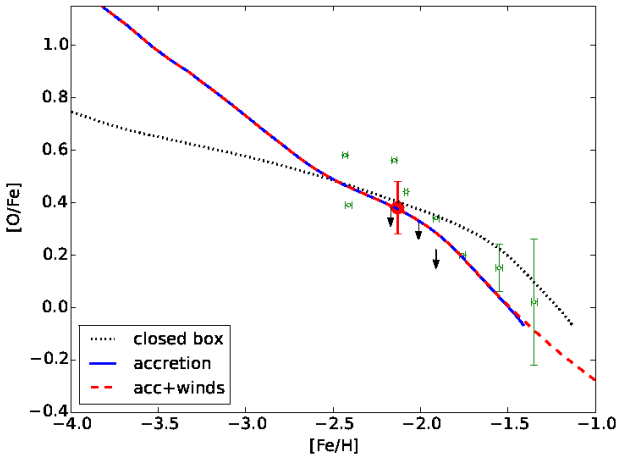


Figure 4. Oxygen abundances in 12 UMi stars . Literature data are taken from Shetrone et al. (2001) (black arrows for the upper limits) and Cohen & Huang (2010) (green dots). Our star is shown with the red filled circle. The chemical evolution models are the closed box (black dotted line), model with 5 Gyr of gas infall (blue solid line) and the model with infall and gas loss through winds (red dashed line).

matching the observed abundance ratios, even though they were not used in fitting the model parameters.

3.1 α-elements: O, Mg, Si, Ti, Ca

The measured α-element abundances (see Fig. 3) are generally consistent with a SF efficiency that is lower than that of the Galactic halo, as also shown by our models which show a gradual de-

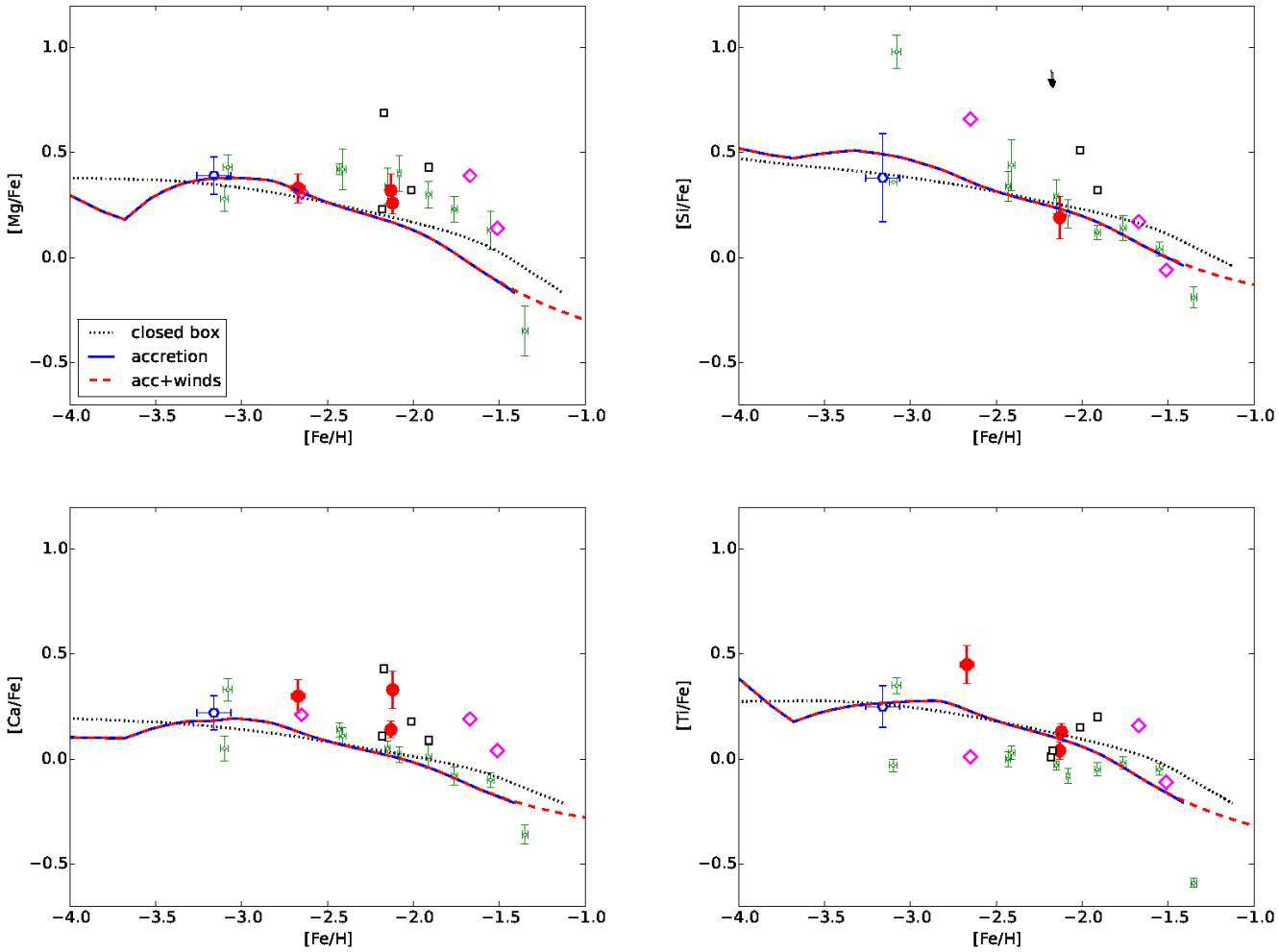


Figure 3. α-elements in UMi. The symbols are data from: this work (red filled circles), Shetrone et al. (2001) (black squares, and arrows for the upper limits) and Cohen & Huang (2010) (green dots), Sadakane et al. (2004) (empty magenta diamonds) and Kirby & Cohen (2012) (blue empty hexagon). The average abundances for these elements in halo stars as calculated by Cayrel et al. (2004) are: [Mg/Fe]=0.26 dex, [Si/Fe]= 0.42 dex, [Ca/Fe]=0.35 dex, [Ti/Fe]=0.26 dex.

crease in the [α/Fe] caused by the onset of SNIa already at very low metallicities (in the models at [Fe/H]= -3). On the other hand, the data for both [Mg/Fe] and [Ca/Fe] indicate a plateau at [Fe/H]$\leqslant -2$ dex though sparsely sampled, which is not found in the models. For the rest of the individual elements, our [Ca/Fe] and [Ti/Fe] abundances, which are closer to Shetrone et al. (2001) and Sadakane et al. (2004) data at higher [X/Fe] values than the Cohen & Huang (2010) data, are only slightly lower than the halo abundances. The [Si/Fe] ratio has a larger scatter in UMi than in the halo (where it is nearly constant), and the [O/Fe] ratio which is reproduced well by our models (see Fig. 4) is lower in UMi than in the halo stars (Cayrel et al. 2004; Cohen & Huang 2010). However, additional lower metallicity stars are needed in order to better distinguish among the different models.

As seen in Fig. 3, model A (without infall and winds), tends to have a less pronounced decrease at higher [Fe/H] which is due to the relatively higher SF compared to models B and C. Concerning these two models, the only difference is that model C (with winds) is able to produce stars at a higher metallicity. This reflects the MDF we obtain for it, driven by the late metal pollution (mostly SN Ia) in a decreasing reservoir of gas which produces a higher concentration of metals. On the other hand, we underline that while the winds do not change significantly the chemical evolution for this galaxy, they help explain the absence of gas at the present time and improve the match with the MDF. Instead of evoking an episodic star formation, our models use an extended, low-efficiency star formation period.

3.2 Fe-peak elements: Sc, Cr, Ni, Mn, Cu, Zn

As seen in Fig. 5, our models generally reproduce the abundances of the Fe-peak elements well. Similarly to the Sadakane et al. (2004) data, our stars have abundances close to those found in halo giants (Cayrel et al. 2004) in Ni and Cr (slightly higher in Zn), and are higher compared to those from Cohen & Huang (2010). The [Cr/Fe] abundance at nearly the solar value in UMI446, UMI718, UMI K from Shetrone et al. (2001) as well as the two more metal rich Sadakane et al. (2004) stars shows a plateau for this element apart from the decline towards lower metallicities which is likely to be caused by NLTE conditions as argued by Bergemann & Cescutti (2010). The Cu abundances we measure in UMI718 and UMI396 are in agreement with the whole UMi sample available to date, which show a decline with increasing metallicity.

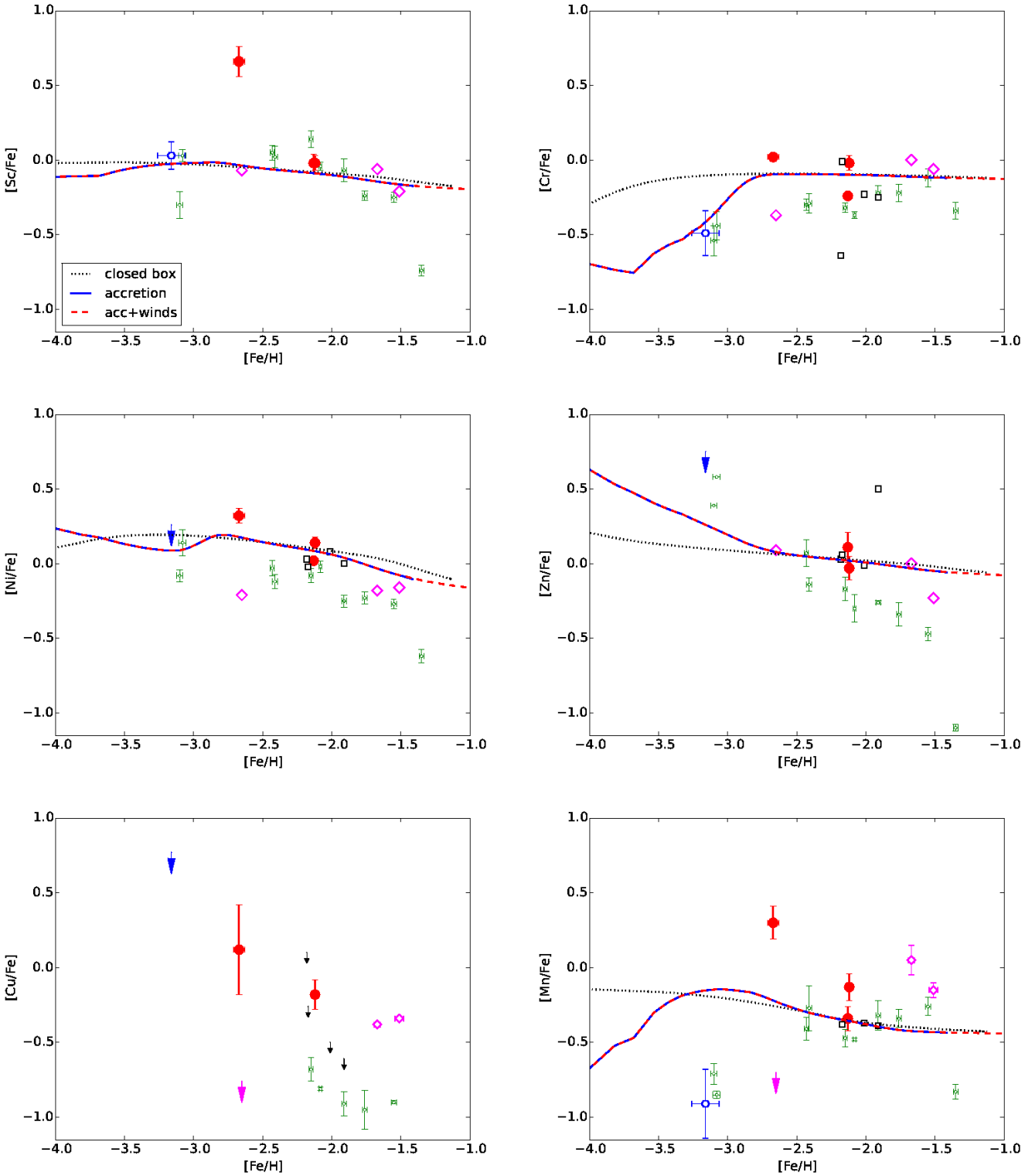


Figure 5. Abundances for the Fe-peak elements. The symbols and colors are the same as in Fig. 3.

For Mn, we match the bulk of the data at intermediate metallicity, so the model is relatively successful, however the decrease predicted at the extremely low metallicities by our models is not consistent with the data in which this signature is detected at [Fe/H]=-3 dex. Our most metal poor star, UMI446, deviates from rest of the data set with a strong enhancement in Fe-peak elements, particularly in Sc and Mn. Although stars measured by Sadakane et al. (2004) display [Mn/Fe]>0 as well, UMI446 has a much lower [Fe/H] than these two, and cannot be explained by our chemical evolution model even if we take into account metal-dependent Mn

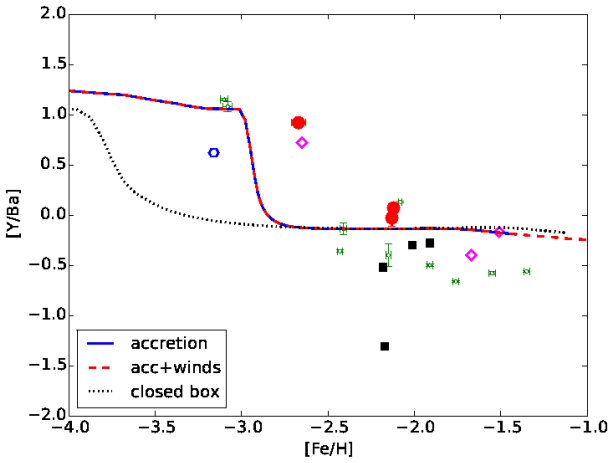


Figure 7. The ratio of yttrium to barium abundances in the UMi stars. The symbols and the colors are as in Fig. 3.

yields for both SNe Ia and SN II as used by Cescutti et al. (2008) and North et al. (2012).

As a final remark in this subsection, we find the chemistry shown by the most metal rich star measured by Cohen & Huang (2010) challenging. An anomalous pollution by SN Ia which cannot be simulated by our simple chemical evolution models, could explain the measured drop in the ratio of α-elements (and neutron capture elements). However, it is more difficult to explain the strong enrichment of Fe in this star without an enrichment of the other Fe-peak elements.

3.3 Neutron capture elements: Y, Ba, Ce, Nd

There are several interesting points that are seen in the neutron capture element abundances in UMi. First, all of the neutron capture elements that we measure have very large scatter across the observed stars, covering a range of about 2 dex. The Y and Ba abundances for the data set are shown in Fig. 6 and the [Ce/Fe] and [Nd/Fe] abundances in two new stars each are given in Table 3. Due to this spread in the observed abundances, we expect that inhomogeneous modeling would be required to obtain a more precise match to the data (see for example Cescutti 2008, Cescutti et al. 2013 and Cescutti and Chiappini 2014). Nevertheless, a simple chemical evolution model should be able to reproduce the mean trend.

The second point of note is the increase of [Ba/Fe] with metallicity seen in the entire UMi sample (Fig. 6) and which overlaps with the halo stars (Fulbright 2000; Cohen & Huang 2010). In Fig. 6, we show that the model results for Y and Ba are in reasonable agreement with the data in that there is a systematically lower average [Ba/Fe] ratio at [Fe/H]$<\lesssim$3 dex compared to higher metallicities. In addition, although the present data in UMi cannot resolve these details, the models predict a dip in both the [Y/Fe] and [Ba/Fe] abundance ratios at [Fe/H]~ -3, which is due to the timescale at which the r-process production by electron capture SN (see Cescutti et al. (2013) for details) starts.

Finally, as predicted by the theoretical nucleosynthesis prescriptions we use, the data show a much lower [Ba/Fe] ratio at very low metallicity, where the [Y/Fe] remains approximately at the same level. At lower metallicity, the production of these neutron capture elements could be sustained by s-process production in fast rotating stars. Note that the low [Ba/Fe] abundance ratio is also found in the Hercules dSph over a broad range in [Fe/H] (Koch et al. 2013) This effect is clearer when we plot the ratio between these two neutron capture elements (see Fig. 7). In this model, before the r-process production starts at [Fe/H]~ -3, the ISM is enriched only through s-process production in spinstars, which is confirmed by an overabundance in [Y/Ba] found in the data at very low metallicities. There is possibly an offset of ~0.5 dex between the last data with high [Y/Ba] defined by UMI446 from this work and COS4 from Sadakane et al. (2004) and the knee found in the model; this can be explained both in terms of inhomogeneity of the system and also in tiny variations in the parameters of the chemical evolution model, definitely inside the uncertainties of our modelling.

4 DISCUSSION

In this paper, we presented a new data set of chemical abundances for the Ursa Minor (UMi) dSph, based on spectra taken with the Keck HIRES spectrograph, as well as a new set of chemical evolution models for 12 elements. A data set combining our new measurements with data from previous studies is consistent with a scenario in which the very metal poor stars in the dSphs have α-element abundances generally comparable to those in the Galactic halo, although in UMi, there is a gradual decrease in the α elements with increasing metallicity which indicates that the ISM was also enriched by SN Ia. The halo stars do not show this trend which is a signature that the star formation in the halo stopped on a shorter timescale compared to the timescale for the enrichment by SN Ia.

Our chemical evolution models use similar nucleoynthesis prescriptions to those by Lanfranchi et al. (2006, 2008) for modeling UMi with the smaller data set available at the time. However, our implementation of the star formation rate is different as we derive the SFH exclusively from the CMD, as done by North et al. (2012) for computing the manganese abundances in four other dSphs. Here, we extended these latter models to study Ursa Minor for the first time and to include the other elements for which we have measured abundances. The most striking novelty in the models is the nucleosynthesis adopted for the neutron capture elements; due to the lack of data, the signature of increasing [Y/Ba] ratio toward lower metallicities was not studied in these previous works. The overabundance of [Y/Ba] at very low metallicity, similar to that found in the Galactic halo, is reproduced by nucleosynthesis in the spinstars as argued in Cescutti & Chiappini (2014) and is modeled for the first time for a dSph. This trend is due to the timescale of the onset of r-process production by electron capture in SN (see Cescutti & Chiappini 2014); before this point the production of the neutron capture elements could be sustained by s-process production in fast rotating stars (Cescutti et al. 2013).

In the ratio of the [α/Fe] abundances, it is not easy to identify the trends in the data, ie. whether these elements show plateaux at low metallicities up to around [Fe/H]$= -2$ dex, or whether they are matched better by a gradual decrease of [α/Fe] starting from very low metallicities as found in our models. In either scenario, together with subsolar values of [Ba/Fe] up to the same metallicity where it reaches the solar value, the abundances are consistent with a SF process that lasted a relatively long time ($\approx$ 5 Gyrs) but had a very low efficiency until it stopped at [Fe/H]=-1.3 dex. While earlier studies found that an inefficient SF in a system without infall or mass loss seemed to fit the data (Ikuta & Arimoto 2002), as the spectroscopic samples grew, already Kirby et al. (2013) were able to show that to obtain the MDF, a model with the infall of gas was

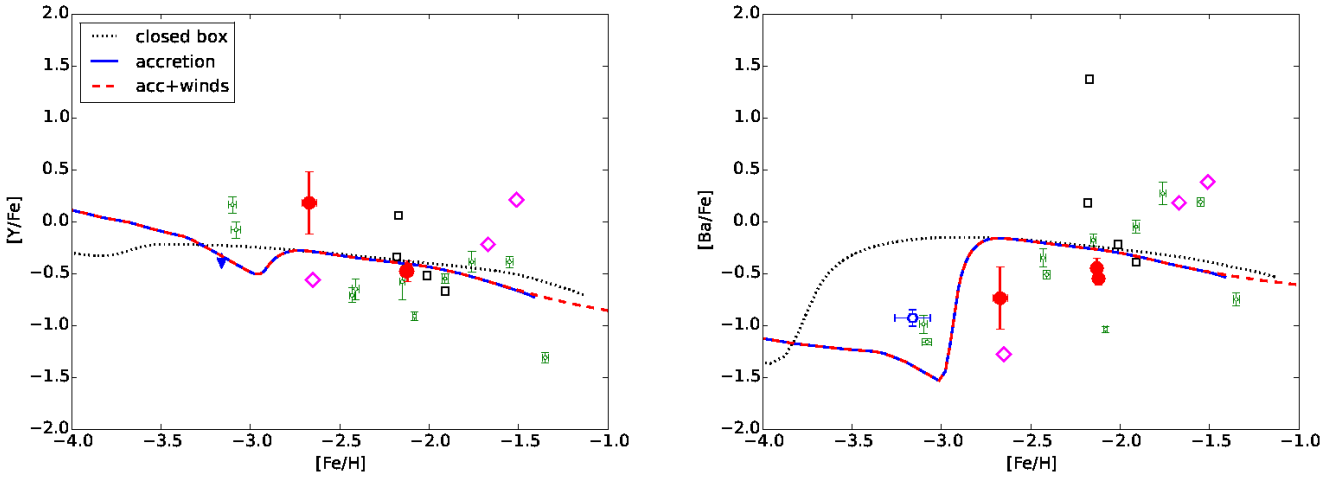


Figure 6. Abundances for the neutron capture elements in UMi giants.The symbols and colors are the same as in Fig. 3

required. Our best model is one where a gas loss proportional to the amount of total gas was also included (winds), and could account for both the low efficiency of the SF at later stages and the observed lack of gas today. We emphasize that, realistically, the gas loss from the dSph is due to a combination of supernova feedback, winds and tidal interactions and hence would have a more drastic effect.

Our results are consistent with the previous data except for a deviation of the abundances of the Fe-peak elements for UMI446 which is our most metal poor star. The [Fe/H] of this star is very similar to COS4 from Sadakane et al. (2004) which has [Fe/H]= −2.7 dex. Although abundances of the low Z α-elements are consistent with the rest of the sample, UMI446 has an unexpectedly higher abundance of Sc and the α-elements Ti and the Fe-peak elements Cr, Mn, Ni, Cu, Zn. At Z=30 it becomes consistent again with the rest of the data, which is especially important in the relation of the [Y/Ba] ratio with metallicity. Among these, one of the most challenging features is the overabundance of Mn for UMI446. These intriguing results could point to an inhomogeneous chemical enrichment of the ISM at the early stages. Although this inhomogeneity would be short lived, it might be able to produce a star like UMI446 if the explosive nucleosynthesis of a SN II through a very massive progenitor with bipolar explosion (jet-like) is taken into account, as suggested by Maeda & Nomoto (2003).

In the future, we plan to investigate the production of the spread in the observed abundances in UMi using more sophisticated, inhomogeneous models to have a clearer insight to its chemical evolution.

5 ACKNOWLEDGMENTS

The data presented herein were obtained at the W.M. Keck Observatory, which is operated as a scientific partnership among the California Institute of Technology, the University of California and the National Aeronautics and Space Administration. The Observatory was made possible by the generous financial support of the W.M. Keck Foundation. MIW acknowledges the Royal Society for support via a University Research Fellowship. AK thanks the Deutsche Forschungsgemeinschaft for funding from Emmy-Noether grant Ko 4161/1.

REFERENCES

Asplund, M., Grevesse, N., Sauval, A. J. et al., ARA&A, 47, 481
Benítez Llambay, A., Navarr J. F., Abadi, M. G. et al., 2014, arXiv:1405.5540.
Bergemann, M., Gehren, T., 2008, A&A, 492, 823
Bergemann, M., Cescutti, G. , 2010, A&A, 522, 9
Carrera, R., Aparicio, A., Martinez-Delgado, D. et al., 2012, AJ, 123, 3199
Castelli, F., Kurucz, R. L, arXiv:astro-ph/0405087
Cayrel, R., Depagne, E., Spite, M. et al., 2004, A& A, 416, 1117
Cescutti, G.,Matteucci, F., Lanfranchi, G. A. et al., 2008, A & A, 491, 401
Cescutti, G. , Chiappini, C., Hirschi, R. et al., 2013, A&A, 553, 51
Cescutti, G., Chiappini, C., 2014, A&A, 565, 51
Cohen J. G., Juang, W., 2010, ApJ, 719, 931
de Boer, T. J. L., Tolstoy, E., Hill, V. et al., 2012, A& A, 544, 73
François, P., Matteucci, F., Cayrel, R., Spite, M., Spite, F. et al., 2004, A& A, 421, 613
Fulbright, J. P., 2000, AJ, 120, 1841
Helmi, A., Irwin, M. J., Tolstoy, E. et al., 2006, ApJ, 651, 121
Hendricks, B., Koch, A., Lanfranchi, G., 2014, ApJ, 785, 102
Ikuta, C., Arimoto, N. 2002, A&A, 391, 55
Johnson, J., 2002, ApjS, 139, 219
Kirby E. N., Cohen J. G., Lanfranchi, G. A. et al., 2011, ApJ, 727, 78
Kirby E. N., Cohen J. G., 2012, AJ, 144, 168
Kirby E. N., Cohen J. G., Guhathakurta, P. et al., 2013, ApJ, 779, 102
Kleyna, J. T., Geller, M. J.,Kenyon, S. J. et al., 1998, AJ, 115, 2359
Koch, A., Grebel, E. K., Wyse, R. F. G. et al., 2006, AJ, 131, 1405
Koch, A., McWilliam, A., Grebel, E. K. et al., 2008, ApJ, 688, 13
Koch, A., CÂt'té, P., McWilliam, A., 2009, A & A, 506, 729
Koch, A., Feltzing, S., Adén, D., Matteucci, F., 2013, A & A, 554, 5
Lanfranchi, G. A., Mateucci, F., Cescutti, G., 2006, MNRAS, 365, 477
Lanfranchi, G. A., Mateucci, F., Cescutti, G., 2006, A & A, 481, 635

Maeda, K., Nomoto, K., 2003, ApJ, 598, 1163
Martin, N. F., Ibata, R. A., Chapman, S. C. et al., 2007, MNRAS, 380, 281
McWilliam, A., Preston, G.,W., Sneden, C., Searle, L., 1995, AJ, 109, 2757
McWilliam, A., Wallerstein, G., Mottini, M., 2013, ApJ, 778, 149
Moore, C. E., Minnaert, M. G. J., Houtgast, J., 1966, NBS, Mono, 61
North, P., Cescutti, G., Jablonka, P. et al., 2012, A&A, 541 , 45
Ramírez, I., Meléndez, J., 2005, ApJ, 626, 465
Sadakane K., Arimoto N., Ikuta C., Aoki W. et al., 2004, PASJ, 56, 1041
Salpeter, E., ApJ, 1955, 121, 161
Schlegel, D. J., Finkbeiner, D. P.,Davis, M., 1998, ApJ, 500, 525
Shetrone, M. D., Côté, P., Sargent, W. L. W., 2001, ApJ, 548, 592
Simon, J. D., Frebel, A., McWilliam, A. et al., 2010, ApJ, 716, 446
Sneden, C. A. 1973, Ph.D. Thesis, The University of Texas at Austin
Stetson, P. B., Hesser, J. E., Smecker-Hane, T. A. 1998, PASP, 110, 533
Tolstoy, E., Irwin, M. J., Helmi, A. et al., 2008, ApJ, 617, 119
Tolstoy, E., Hill, V., Tosi, M., 2009, ARA& A47, 371
Vogt, S. S., Allen, S. L., Bigelow, B. C., 1994, SPIE, 2198, 362
Walker, Matthew G., Mateo, M., Olszewski, E. W., 2009, AJ, 137, 3100
Wilkinson, M. I., Kleyna, J. T., Evans, N. W., 2004, ApJ, 611, 21.